

PPPL-3162 - Preprint Date: May 1996, UC-420, 421, 426

MEASUREMENT OF ELECTRON ENERGY DISTRIBUTION
FROM X-RAY DIAGNOSTICS - FOIL TECHNIQUES
USED WITH THE HARD X-RAY CAMERA ON PBX-M.*

S. von Goeler, R. Bell, S. Bernabei, W. Davis, H. Fishman[†], D. Ignat, S.
Jones¹, R. Kaita, G. Petravich², P. Roney, J. Stevens³

*Plasma Physics Laboratory, Princeton University, Princeton New Jersey
08543, USA*

¹ Center for Space Research, Massachusetts Institute for Technology, Cambridge, MA 02139, ² CRIP, Budapest,
Hungary, ³ Sandia National Laboratories, Albuquerque, NM 87185-1077, [†]deceased

ABSTRACT: A half-screen foil technique is used with the Hard X-ray Camera on the PBX-M tokamak to determine the energy distribution of the suprathermal electrons generated during lower hybrid current drive. The ratio of perpendicular to parallel temperature of the suprathermal electrons is deduced from the anisotropy of the bremsstrahlung emission utilizing Abel inversion techniques. Results from lower hybrid current drive discharges are discussed.

*) Presented at the 7th International Toki Conference on Plasma Physics and Controlled Nuclear Fusion, "Fusion Plasma Diagnostics", Nov. 28 - Dec.1 1995, Toki-city, Japan

1. Introduction.

The aim of the Lower Hybrid Current Drive (LHCD) experiment on the Princeton Beta Experiment-Modification (PBX-M) tokamak has been to modify the radial plasma current profile in order to find advanced tokamak configurations. [1],[2] The interaction between the lower hybrid waves and the plasma electrons leads to the formation of suprathermal electrons, which are thought to be ultimately responsible for the current drive. [3] On PBX-M, the suprathermal electrons are diagnosed by the Hard X-ray Camera (HXC), [4],[5] that acquires tangential images of the bremsstrahlung emission generated in collisions of the hot electrons with plasma ions. This emission typically ranges in energy from ten to several hundred keV. This paper describes the techniques that we use to measure the energy of the suprathermal electrons, and summarizes our present knowledge of the energy distribution of the suprathermal electrons during lower hybrid current drive.

2. Hard X-ray Camera and Half-Screen Foil Technique.

LHCD experiments were pursued on PBX-M over two run periods in 1992 and in 1993. After the 1992 run, a number of technical improvements were made on the HXC. Since the HXC has already been discussed extensively in Ref. 4 and 5, we will provide only a very short description of it here, with an emphasis on the upgrades. A schematic layout of the HXC (as of the 1992 run) is shown in Fig. 1. The pinhole camera views the plasma tangentially. The field of view is chosen so that it includes (a) the outermost plasma radius, determined by an

outside limiter, and (b) a region beyond the pusher coil. Region (a) is essential for performing Abel inversions, while region (b) is important because the sight lines viewing it have a large inclination with respect to the magnetic field, and thus permit a more accurate determination of the anisotropy of the emitted bremsstrahlung radiation. Hard X-rays from the plasma enter the camera through a lead pinhole aperture and strike the 9" diameter scintillator screen of an X-ray image intensifier (Hamamatsu Model VP2465P). The X-rays generate light pulses in the scintillator screen that lead to electron emission from a thin photocathode that is evaporated on the scintillator. The photo electrons are accelerated to 30 keV and imaged on a 21.4 mm phosphor screen.

The most important improvement for the 1993 operating period was made in the foil drive. In the 1992 run, we inserted a foil close to the aperture between shots, and compared the X-ray intensity from consecutive shots. Most of the foil data obtained this way turned out to be unusable, because discharges were not reproducible enough, and small differences in plasma density can cause large changes in the hard X-ray emission (i. e. in the density of suprathermal electrons). The variations in X-ray intensity due to irreproducibility were comparable to the changes generated by inserting the foils. It was also observed that the up-down symmetry of the images was well-conserved, i. e., the top half of the image mirrored the bottom half and the mirroring axis did not change in discharges of the same type. Therefore, we built a new foil drive (Fig. 2), where a molybdenum and a copper foil cover only the top or bottom half of the image. The foils are moved from the open to the closed position by two small double-acting air cylinders.

Fig. 3 illustrates how the foil data were evaluated. The raw data for shot 309274 are represented by the heavy solid line. This curve represents a verti-

cal profile from one of the 64 HXC frames taken during the shot, i. e., the average of 5 pixel columns that go directly through the center of a hollow discharge. The large sudden dips in the curve at pixel 27, 62 are due to a lead wire grid in front of the tube that allows us to check that the magnetic field of the tokamak has not distorted the image. The following plasma shot #309275 was taken without foil and serves as reference. A double Gaussian (the dashed curve) is fitted to the profile of the reference shot, and the location of the mirroring axis (pixel 46 for Fig. 3) is determined. It depends on the vertical plasma position. The top half of shot 309274 is then mirrored on the bottom half and smoothed slightly to remove the dips caused by the lead grid.

Clearly a region around the mid plane has to be excluded because the projection of the edge of the foil - determined by mechanical construction - does not normally coincide with the mirroring axis that varies as the plasma evolves. In addition, simulation of the HXC images (Fig. 11 in Ref. [7]) has shown that there can be up-down asymmetries in the image that stem from helical effects. The asymmetries occur when the hot electrons are very energetic and anisotropic. It seems, however, that these effects do not play a large role for typical LHCD conditions on PBX-M, where the hot electron temperature is usually less than or equal to 100 keV. Furthermore, any up-down asymmetries would have been noticed, since numerous reference shots were taken regularly.

3. Photon Temperature and Hot Electron Temperature.

From the foil measurements, we determine the photon temperature. [6,7] The two mirrored curves of Fig. 3 yield the X-ray intensities I_{Cu} and I_{nf} with and without copper foil. A vertical profile of the photon temperature, Fig. 4, is obtained using the formula

$$T_{photon} = \frac{E_{cut-off\ Cu} - E_{cut-off\ nf}}{\ln(I_{nf}) - \ln(I_{Cu})},$$

where $E_{cut-off\ nf}$ and $E_{cut-off\ Cu}$ are the low energy cut-off values (i. e., the energy were $\Sigma \mu d = 1$ for all the absorbing material in the X-ray path). For the HXC on PBX-M, the nf and Cu cut-off energies were 45 and 65 keV, respectively. The relatively high value for the no-foil cut-off is due to the 3 mm-thick aluminum vacuum flange on the PBX-M port and two connectic magnetic shielding foils in front of the X-ray image intensifier tube.

The vertical T_{photon} profile in Fig. 4 displays a peak of 34 keV in the plasma center, has a minimum of 24 keV about half way out, and increases then steeply to 62 keV near the plasma edge. The increased photon temperature near the plasma edge has been often observed earlier [7, 8, 9]. For some discharges, however, the temperature increase near the edge does not occur. No systematic study has been made under what conditions the increase occurs. We would like to point out that the photon temperature measurement becomes very inaccurate when the photon temperature is high, because under these circumstances the difference between the Cu and the nf intensity profile becomes small. This is particularly true near the edge where the intensity is small and statistical noise and background are large.

The next step is to obtain the energy of the suprathermal electrons from the photon temperature. It should be stressed that the photon temperature, as we have defined it, does not represent the reciprocal slope of the emitted photon spectrum, but is only related to it, because the efficiency of the X-ray image converter tube was not properly taken into consideration. This problem is solved by using the PBXRAY [6] code to simulate images for the nf and the Cu case. Photon temperatures from the simulated images are then calculated with the same algorithm used to obtain the experimental photon temperature data. Results for the three temperature model, [8] where the momentum distribution function has a Gaussian shape determined by three parameters, the parallel forward temperature T^f , the parallel backward temperature T^b , and the perpendicular temperature T^\perp , are shown in Fig. 5. The four curves represent horizontal profiles of the photon temperature for four sets of hot electron temperatures. For each set the ratio between parallel and perpendicular temperatures was kept constant, i. e. $T^f = 4 T^\perp$ and $T^\perp = T^b$. The figure suggests that the hot electron temperature in the hollow ring of shot 309274 is about 80 keV, and that it probably exceeds 500 keV near the plasma edge, within the uncertainties discussed earlier.

4. Abel Inversion with Anisotropic Emission.

For the interpretation of the HXC images, we have developed a simulation code [6] and two inversion codes [10] and [11]. The new and interesting feature of the two inversion codes is that they take into consideration the anisotropy of the hard X-ray emission. While the 2D method [10] is probably the more accurate of the two, it has two drawbacks. First, it requires knowledge of the equilibrium configuration for each point in time, and thus depends on a fast

equilibrium solver that was not available during the analysis. The second disadvantage is that an a priori assumption has to be made about the density distribution of suprathermal electrons on a magnetic surface, usually a $1/R$ dependence. [12]

The 1D method [11] performs the inversion in the horizontal mid plane only, where the magnetic surfaces can be represented by concentric circles, and no calculation of the equilibrium is required. The only assumption made about the hot electron density is that it does not vary with toroidal angle. The bremsstrahlung emissivity is assumed to be the product of a function $\epsilon(R)$ of the major radius R and - because of the anisotropy - a function $F(\theta)$ of the angle θ between the magnetic field line and the line of sight. For the very low-energy hot electrons encountered during LHCD, the direction of the field line can be approximated by a tangent to the concentric circle. We calculate $F(\theta)$ from the Stevens code [8] using the three temperature model. Typical examples are given in Fig. 6 for the no-foil case. The left half of Fig. 6 shows a series of $F(\theta)$ curves where the energy of the hot electrons (T^{\wedge}_f) was varied from 40 to 400 keV while the anisotropy was kept constant ($T^{\wedge}_f = 4 T^{\wedge} = 4 T^{\wedge}_b$). The right half of Fig. 6 shows a series where the anisotropy was varied by changing $T^{\wedge} = T^{\wedge}_b$ from 10 to 100 keV while the energy was kept constant ($T^{\wedge}_f = 100$ keV). For the hollow discharges with -90° LH phasing, the forward parallel temperature is known to be 100 keV from foil measurements. In Fig. 7, we show inversions where the perpendicular temperature is varied from 10 to 100 keV. The Abel-inverted intensity can not become negative in the region before the pusher coil. Therefore the Abel inversion indicates that T^{\wedge} equals 10 ... 25 keV. This result agrees with a previous analysis using the simulation code. [6]

5. Lower Hybrid Power Deposition.

As an application of the foil techniques, we want to discuss now HXC data (Fig. 8) that were obtained during three LH phase scans undertaken to study LH wave physics. In each of the three subfigures, four quantities are plotted: (1) radial location (minor radius in the horizontal mid plane) of the maximum of the Abel-inverted hard X-ray profile (for hollow discharges), (2) radial location of the half maximum on the outside gradient, (3) the measured hot electron temperature from foil measurements, and (4) the maximum hard X-ray intensity in relative units. The data in Fig. 8a were taken at a comparatively high density ($n_e = 1.9 \times 10^{13} \text{ cm}^{-3}$) and high magnetic field ($B = 1.77 \text{ T}$) and have hollow hard X-ray profiles. Fig. 8b, taken at even higher density ($n_e = 2.6 \times 10^{13} \text{ cm}^{-3}$) but much lower magnetic field ($B = 1.33 \text{ T}$), shows even greater hollowness. Fig. 8c, taken at comparatively low density ($n_e = 1.1 \times 10^{13} \text{ cm}^{-3}$) and medium high field ($B = 1.47 \text{ T}$), displays centrally-peaked profiles.

The data exhibit a number of trends, for instance: (a) HXC profiles are hollow at high density and peaked at low density, (b) radius of the maximum increases when the magnetic field is lowered and when the absolute value of the LH phase angle decreases, (c) photon temperature, i. e., the suprathermal electron energy, decreases with increasing LH-phase. These trends agree, not only qualitatively but also approximately quantitatively, with the predictions for classical accessibility of lower hybrid waves. For instance, the radius of maximum X-ray emission corresponds approximately to the radius to which the waves can penetrate in first path absorption. Or, the measured hot electron energy corresponds roughly to what one would expect from the phase velocity of the LH waves at the launching antenna. This, however, is a very puzzling result, because the most recent theories for LH wave propagation [13],[14],[15],

in which LH waves make several bounces and passes through the plasma, are in contradiction with the experimental results. In the regime, a considerable n^{\prime} upshift occurs, and the upshifted waves can penetrate into the interior of the plasma, albeit at lower energy. A clue to the puzzle might be that the HXC on PBX-M has a very high low-energy cut off (45 keV), so it is possible that the lower-energy hot electrons resulting from the upshifted wave are not recorded by the camera. Indeed, recent results from the Tokamak de Varennes [16] showed that - under very similar plasma conditions - the 20-40 keV X-rays had a peaked profile, whereas the 80 - 100 keV profile was hollow. These measurements were performed, however, with an X-ray diagnostic having only a perpendicular view.

6. Hot Electron Collisionality.

Fig. 9 shows HXC data from a discharge with modulated LH power. Similar data were used extensively by Steve Jones to study the hot electron transport [10]. Plotted is the hard X-ray intensity as a function of time for several groups of pixels, with the location indicated in the upper right hand corner. The upper plot is for pixels that were not covered by a foil (total low energy cut-off of 45 keV), and the lower plot presents data from a scintillator screen area covered by a .95 mm molybdenum foil (total low energy cut-off of 115 keV). The thick solid lines is from the central area, the thin solid line is from an area half way out close to the maximum emission, and the dotted lines are from the outer plasma regions.

The no-foil data show that the discharge is hollow during the LH heating, and then makes a transition to a peaked state after the LH power is switched off. At

that time the X-ray intensity drops precipitously, probably because of collisional slowing down and radial diffusion of hot electrons. However, the Mo foil data indicate that there exists a group of high energy electrons (>100 keV) that do not slow down (and that also do not seem to diffuse outward). These very energetic electrons are formed during the LH heating in the center of the plasma - perhaps in a LH-assisted runaway process - and they seem to accumulate after each LH power pulse. They eventually dominate the discharge. What Fig. 9 then shows is that there are two groups of electrons in the plasma with different collisionality, and their very different behavior makes the interpretation of no-foil data difficult, if they are considered alone.

7. Asymmetric Inverted Profiles.

Fig. 10 shows three consecutive Abel-inverted profiles, which exhibit a strange anomaly that has been seen on occasion in PBX-M. Frame #5, similar in shape to the Abel inverted profiles of Fig. 7, is considered a normal hollow profile: the left maximum is slightly larger than the right maximum. This profile shape is understandable, because we expect the density of suprathermal electrons n_{se} to vary as $1/R$ for collisionless passing particles with no perpendicular energy, since their parallel velocity does not change as they move around the torus and since the particle flux in a magnetic flux tube should be approximately conserved. Passing particles with appreciable perpendicular velocity move faster on the outside of the torus, and their density should consequently fall off even faster than $1/R$.

The profiles for frame #6 and #7 are puzzling, however, because in this case the outside maximum is appreciably larger than the inside maximum. We do

not know the reason for the anomaly. It could be that the right-left asymmetry seen in frame #6 and #7 is caused by trapped electrons, an exciting prospect, since it would represent the first X-ray imaging of trapped electrons. However, the hard X-ray emission depends not only on the density and velocity distribution of suprathermal electrons, but also on the density of impurity ions, and it could also be an impurity effect. There is no indication from other diagnostics that some plasma event consistent with our observation occurred at that time. These asymmetries were discovered during the late stages of the 1993 PBX-M run, and really need more experimentation. We feel that the anomaly shown in Fig. 9 is not an artifact of the HXC measurement, but may shed some light on the most difficult problem that we encounter in the analysis of suprathermal electrons, namely determination of the spatial distribution of hot electrons on a magnetic surface.

8. Conclusions.

The bremsstrahlung emitted by suprathermal electrons during lower hybrid current drive is recorded by the PBX-M Hard X-ray Camera for the diagnosis of the hot electron velocity distribution. A half screen foil technique is used to determine the energy (T_e) of the hot electrons from the slope (T_{photon}) of the X-ray spectrum. The measurement is performed during a single shot, alleviating reproducibility problems. The ratio of parallel to perpendicular electron energy ($T_{\parallel} / T_{\perp}$) is determined from comparison of the X-ray emission parallel to the magnetic field to the emission at a large angle to the field. The actual procedure consists of a generalized Abel inversion of the anisotropic bremsstrahlung emission.

Several applications of the foil measurements and the Abel inversion techniques are discussed. The LHCD produces hollow discharges, where the bremsstrahlung emission is not peaked in the center but displays a hollow profile in minor radius, a result that indicates off-axis current drive. The data of Sect. 5 show the variation of the radial location r_{\max} of the hot electron ring and the energy of the hot electrons with the phasing of the lower hybrid grill antenna. These data are important for understanding the LH wave physics. In a different application, the LH power is modulated and the decay of the bremsstrahlung emission after the turn-off of the LH is analyzed. Much shorter decay times are observed for the softer unfiltered bremsstrahlung than for the harder Mo-filtered X-rays. We think that the different decay times reflect the change in collisionality of electrons below and above 100 keV in PBX-M LH discharges.

From the Abel inversion of hollow profiles, a comparison of the inside and outside maximum provides the unique possibility to record the X-ray emission from two points on the same magnetic surface without having to locate the surface very precisely. Most of the inverted profiles have a $1/R$ dependence, approximately, as one would expect for passing particles, but there are a few highly asymmetric profiles, where the outer maximum is much larger than the inner one, indicating the possible presence of trapped hot electrons.

This wealth of information has been obtained during two short run periods on PBX-M, and some of the data analysis is preliminary. The measurements illustrate, however, that the Hard X-ray Camera is a unique and versatile tool to explore the intricate physics of suprathermal electrons.

Acknowledgment: Work supported by Department of Energy Contract NO. DE-AC02-76-CHO-3073. The support of Drs. M. Okabayashi and N. Sauthoff is gratefully acknowledged. Mr. J. Gorman designed and assembled the foil drive.

References

- [1] M. S. Chance, et al.: Phys. Rev. Lett **51**, p. 1963 (1983)
- [2] R. Grimm, M. Chance, A. Todd, et al.: Nuclear Fusion **25**, p. 805 (1985)
- [3] S. von Goeler, J. Stevens, C. Karney, et al.: Proc. 5th Topical APS Conf. on Radio Frequency Plasma Heating, Madison, p.96 (1983)
- [4] R. Kaita, S. von Goeler, S. Sesnic, et al: Rev. Sci. Instrum. **61**, p. 2756 (1990)
- [5] S. von Goeler, S. Jones, R. Kaita, et al.: Rev. Sci. Instrum. **65**, p. 1621 (1994)
- [6] S. von Goeler, H. Fishmann, D. Ignat, et al.: Phys. Plasmas **2**, p. 205 (1995)
- [7] S. von Goeler, S. Bernabei, W. Davis, et al.: Proceeding of the 10th Topical Conference on Radio Frequency Power in Plasmas, Boston, AIP Conf. Proc. 289 (American Institute of Physics, New York, p. 123 (1993)
- [8] J. Stevens, S. von Goeler, S. Bernabei, et al.: Nucl. Fusion **25**, p. 1529 (1985)
- [9] S. von Goeler, J. Stevens, S. Bernabei, et al.: Nucl. Fusion **25**, p. 1515 (1985)
- [10] S. Jones, J. Kesner, S. Luckhardt, et al: Phys. Plasmas **2**, p. 1548 (1995)
- [11] R. Bell: Rev. Sci. Instrum. **66**, p. 558 (1995)
- [12] S. von Goeler, N. Asakura, R. Bell, et al.: Proceedings of the 19th EPS Conf. on Contr. Fusion and Plasma Physics, Innsbruck, Vol. II, p.949 (1992)
- [13] D. Ignat, E. J. Valeo, S. C. Jardin: Nucl. Fusion **34**, p.837, (1994)
- [14] P. T. Bonoli et al.: Nucl. Fusion **28**, p. 991, (1988)
- [15] H. Takahashi, Phys. Plasmas **1**, p. 2254, (1994)
- [16] Y. Peysson, P. Brooker, R. Arslanbekov, et al.: Bull. APS **40**, p. 1714 (1995)

Figure Captions.

Fig. 1: Mechanical layout of the Hard X-ray Camera (HXC) on PBX-M.

Fig. 2: New foil drive mounted on the hard X-ray imaging tube.

Fig. 3: Mirroring of profiles for the determination of the photon temperature.

Fig. 4: Vertical photon temperature profile.

Fig. 5: Modeling of horizontal photon temperature profiles with the PBXRAY code.

Fig. 6: Anisotropy function $F(\Theta)$ for the no-foil case for various values T^{\wedge}_f , T^{\wedge} , T^{\wedge}_b .

Fig. 7: Abel inversion of anisotropic plasmas to determine T^{\wedge} .

Fig. 8: Lower hybrid phase scans for (a) high magnetic field and high density, (b) low field and high density, and (c) low density.

Fig. 9: HXC data with and without molybdenum foil for modulated LH power.

Fig. 10: Abel inverted hard X-ray profiles with large outward asymmetry.

HARD X-RAY CAMERA ON PBX-M

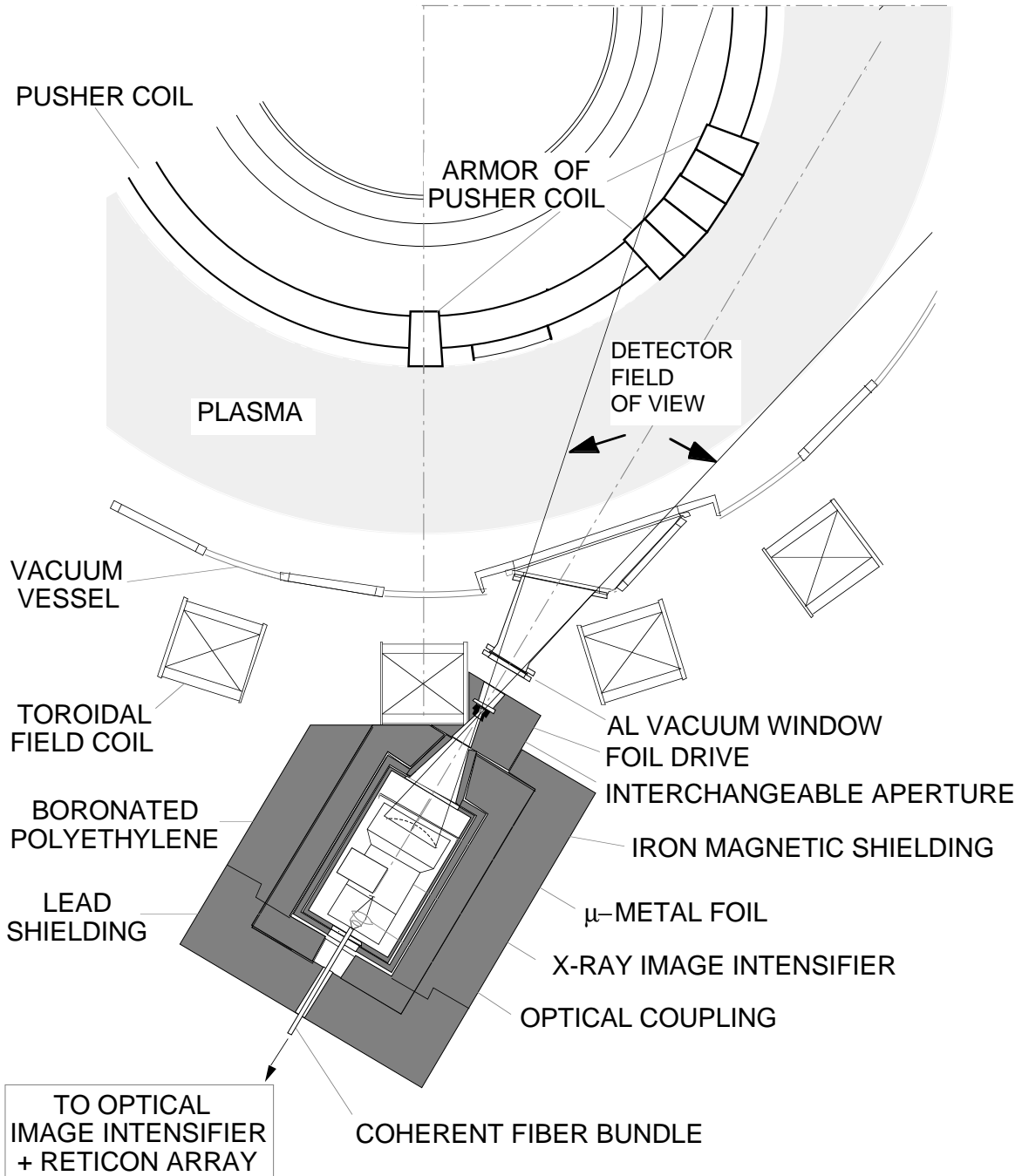


Figure 1



Figure 2

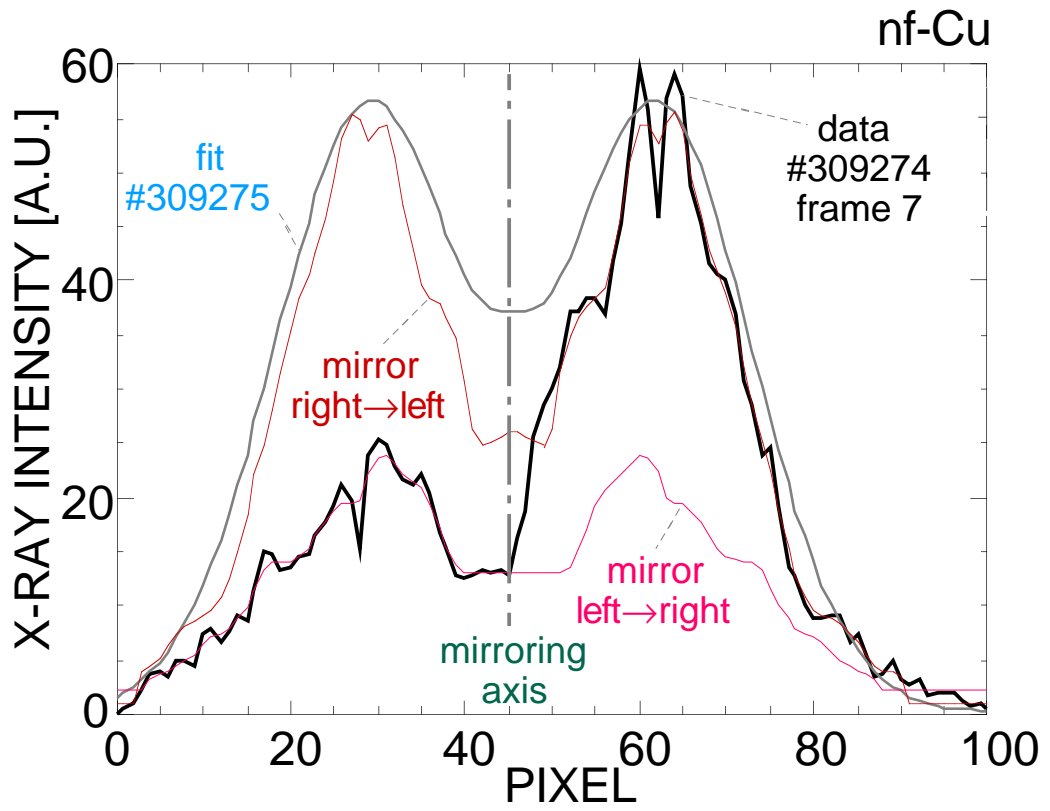


Figure 3

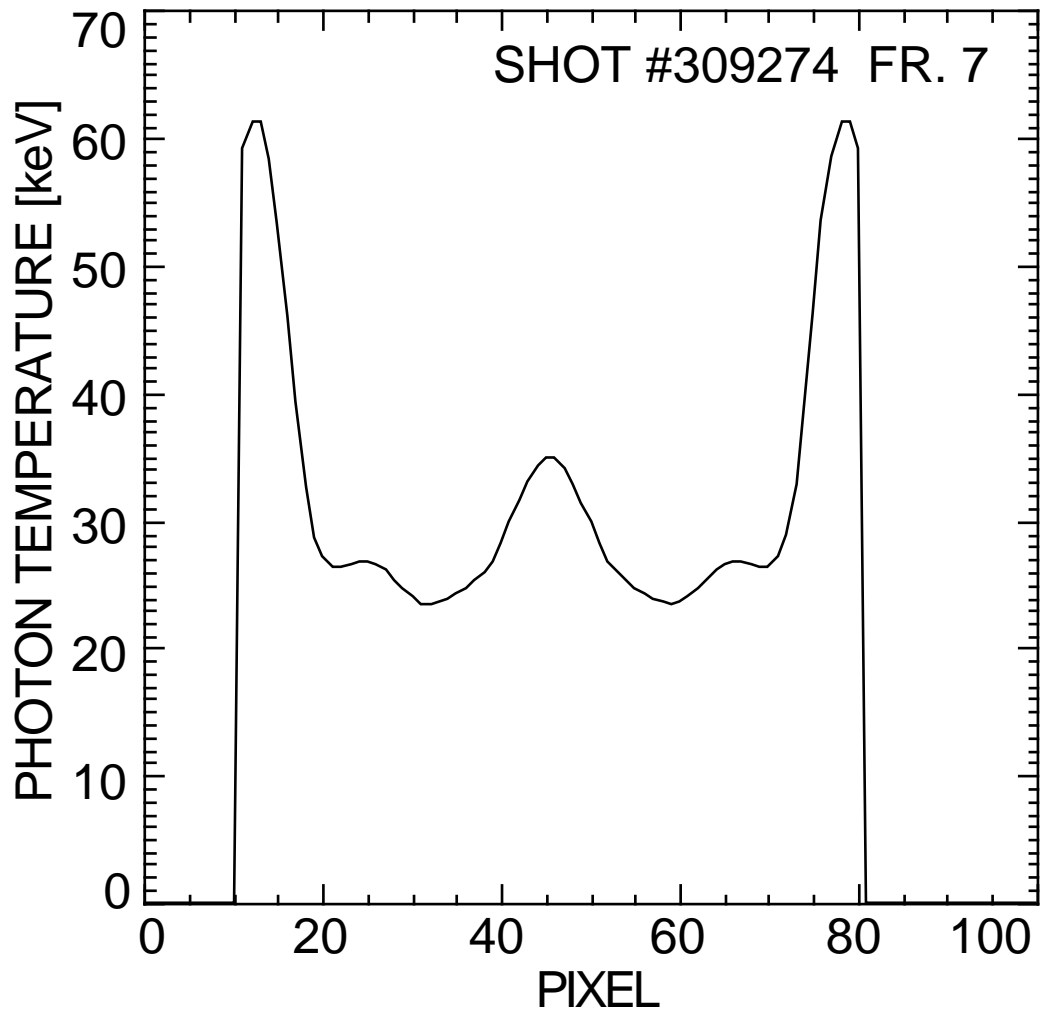


Figure 4

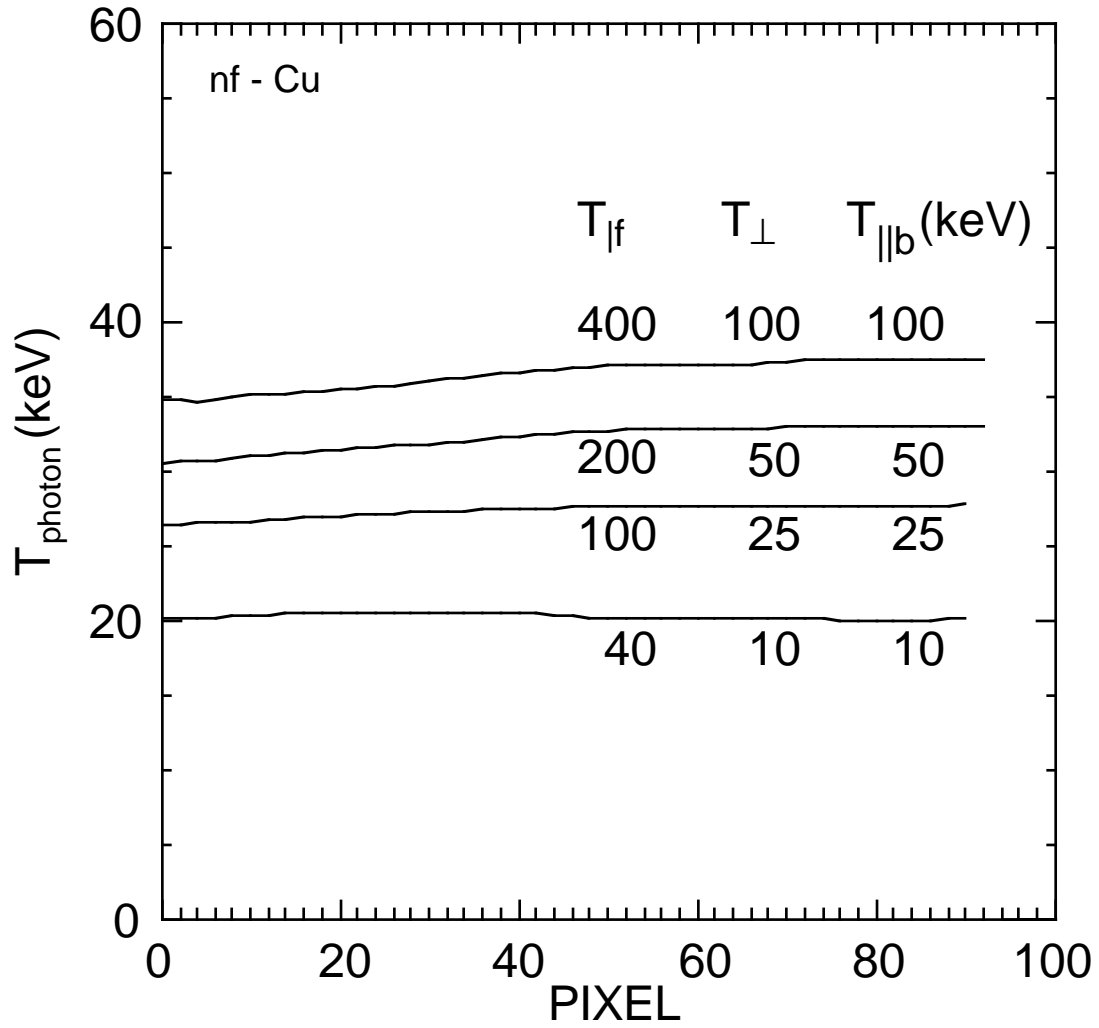


Figure 5

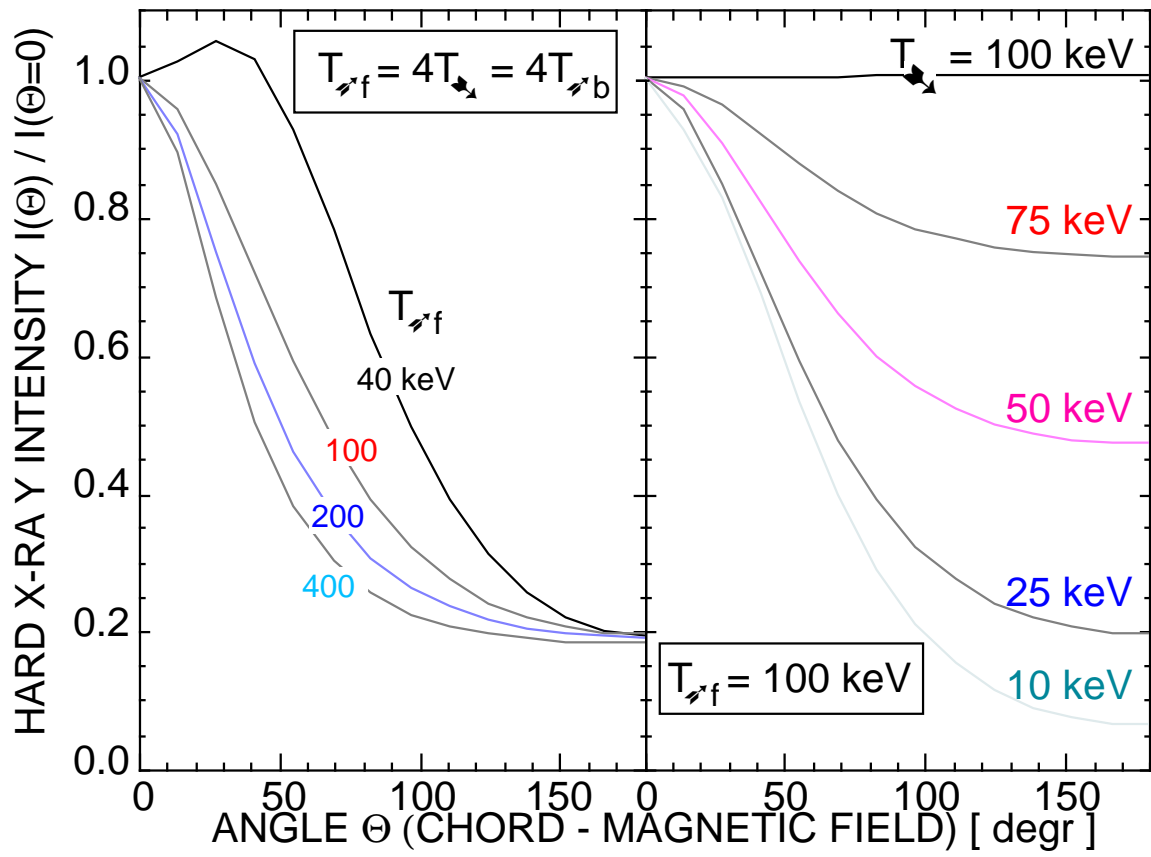


Figure 6

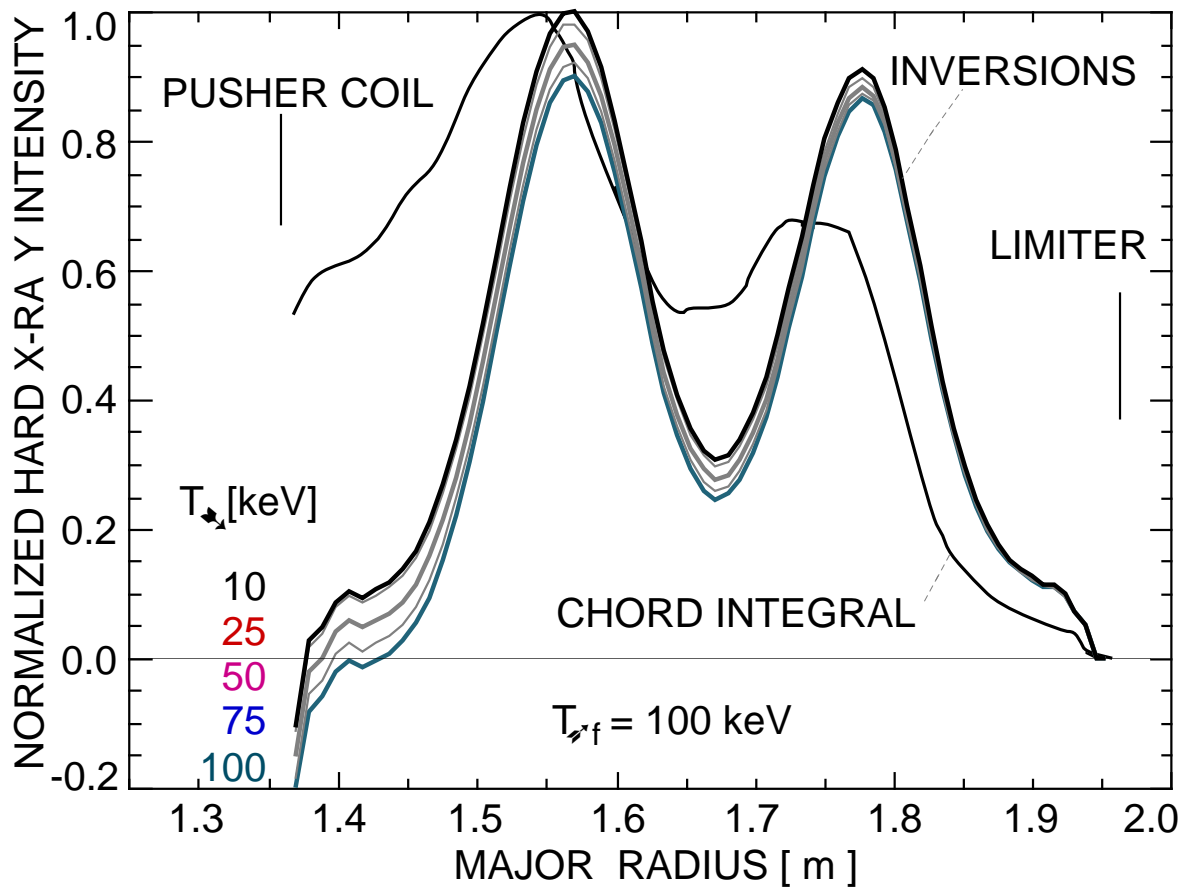


Figure 7

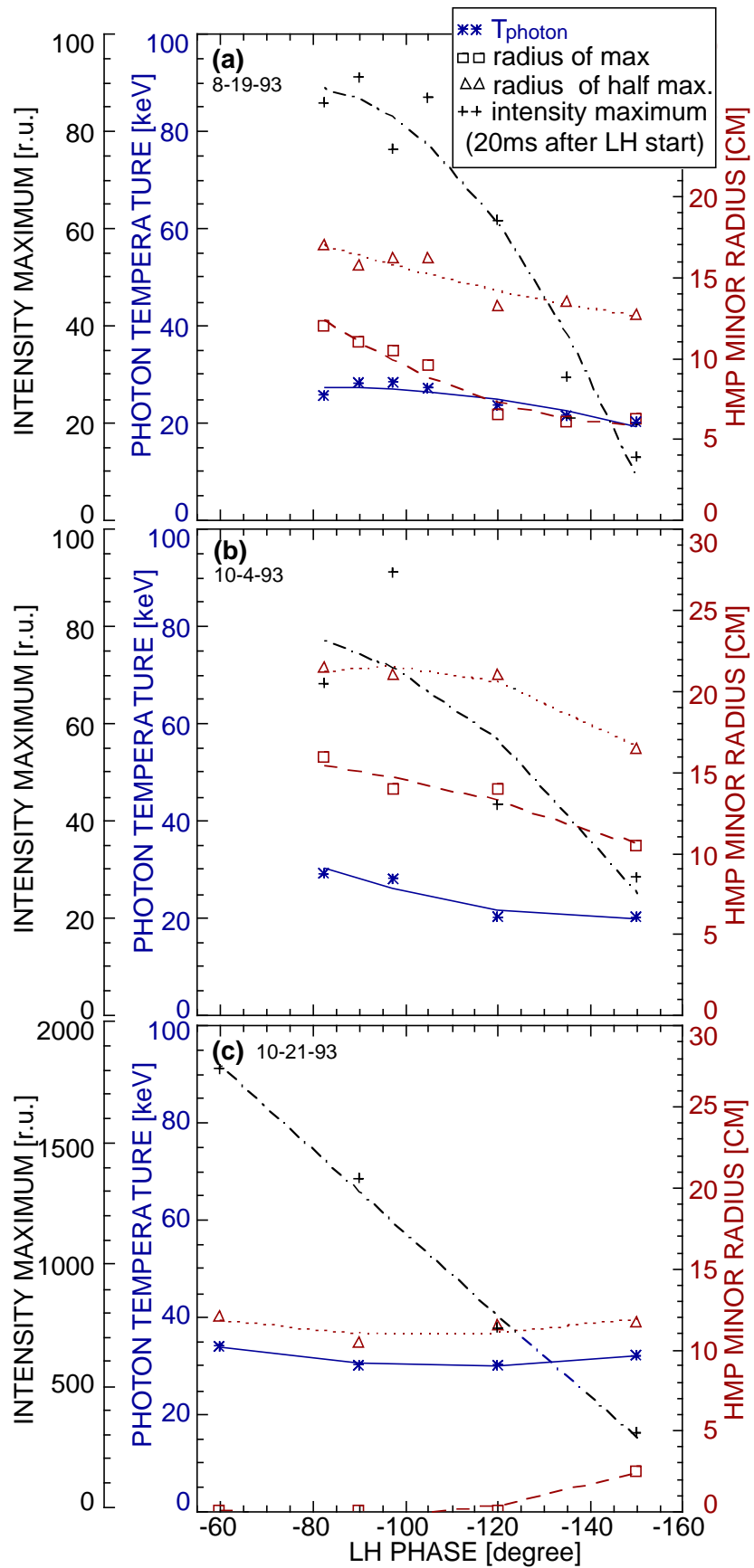


Figure 8

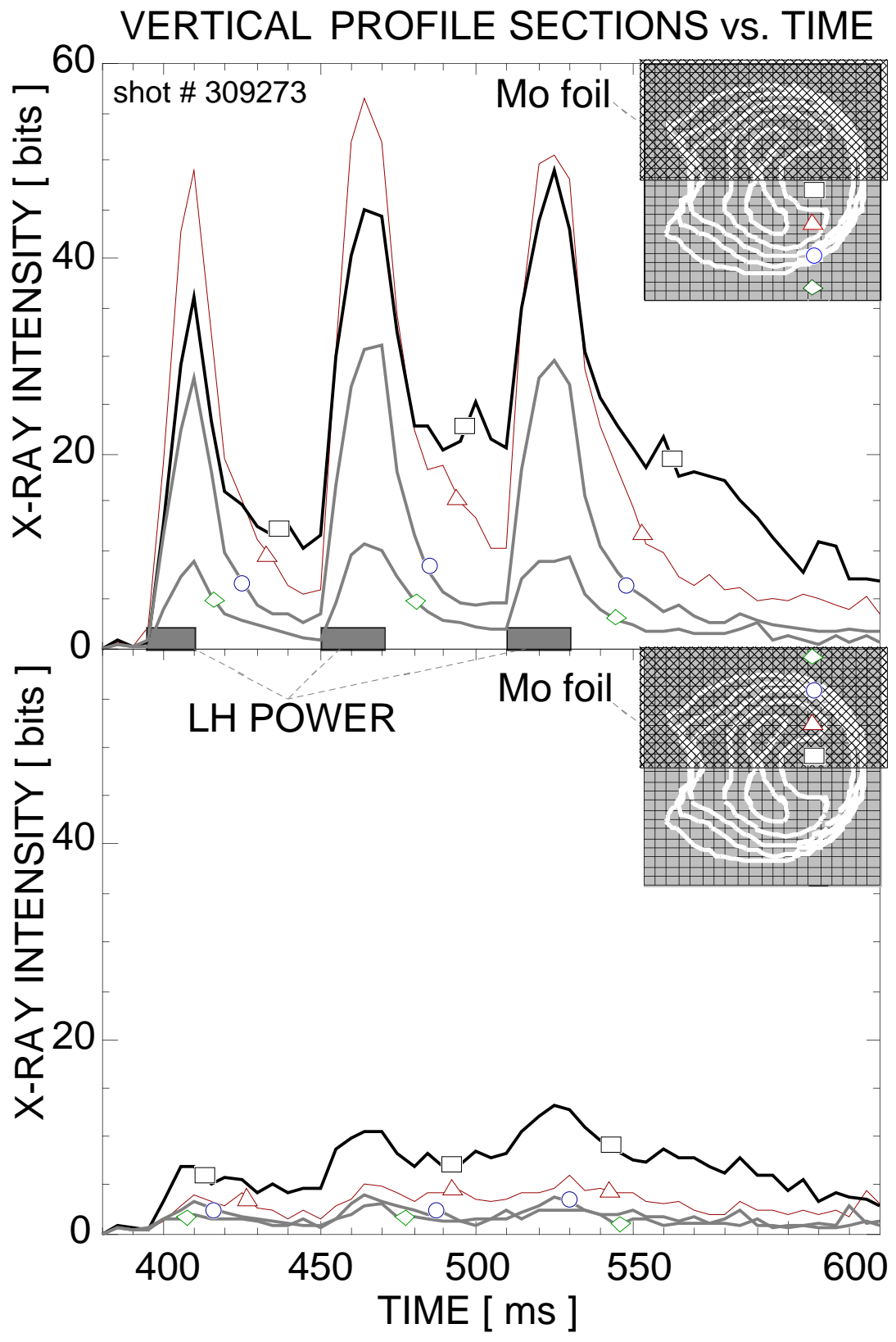


Figure 9

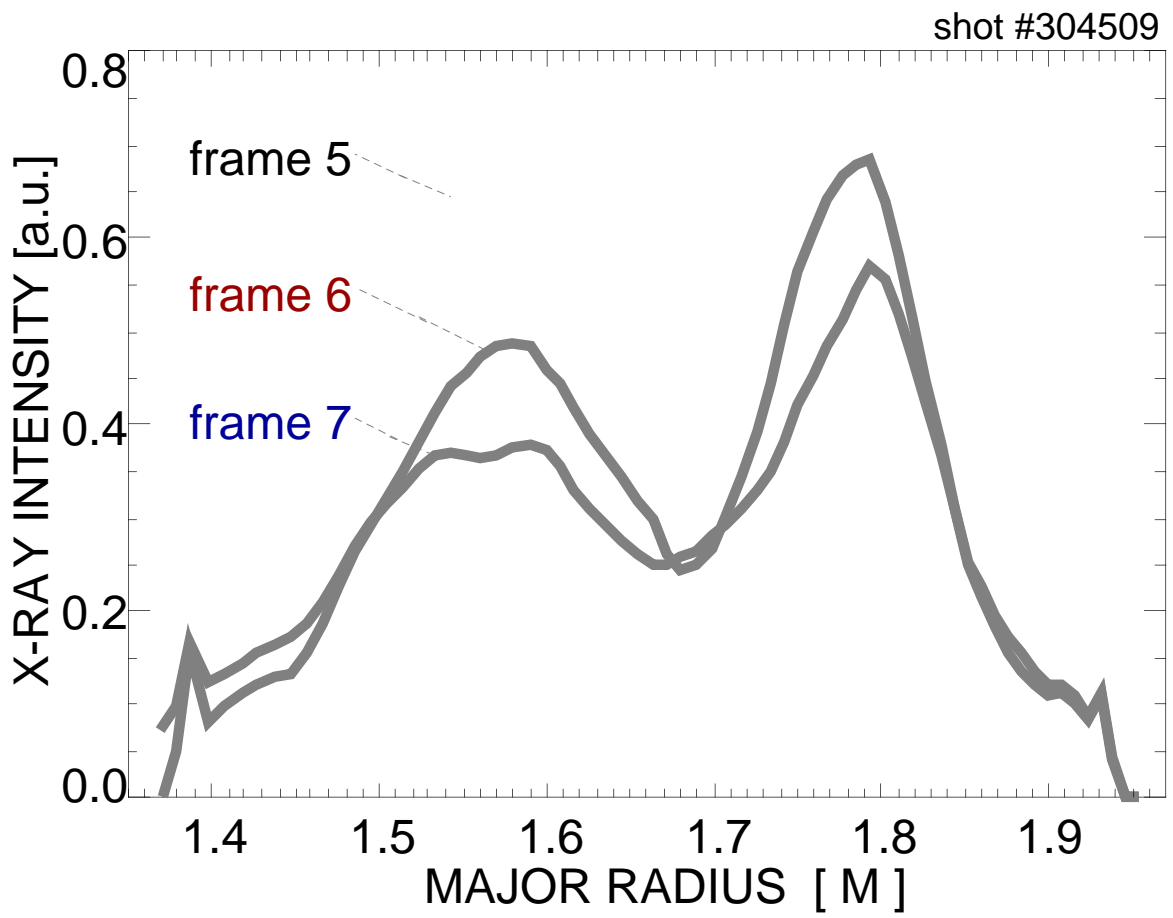


Figure 10